18

Spark-induced breakdown spectroscopy: a description of an electrically generated LIBS-like process for elemental analysis of airborne particulates and solid samples

Amy J. R. Hunter and Lawrence G. Piper
Physical Sciences Inc., USA

18.1 Introduction

Spark-induced breakdown spectroscopy (SIBS) is a plasma-based atomic emission analytical technique that draws from both traditional spark spectroscopy and laser-induced breakdown spectroscopy (LIBS). Like traditional spark spectroscopy, the plasma is formed electrically. Like LIBS, the sparks are generally made in ambient air and detection is timed to eliminate the initial very bright breakdown. SIBS has been applied to a variety of interesting and challenging analytical problems. This chapter describes the basic hardware required to perform SIBS analyses. Here we also present the application of SIBS to real-time monitoring of airborne microparticulate lead in workplace hygiene scenarios, and the use of SIBS as a field-screening analyzer for metal contamination in soils.

SIBS can be regarded as a "marriage" of two other pulsed plasma techniques for elemental analysis: laser-induced breakdown spectroscopy and traditional spark spectroscopy. The latter is generally performed upon conductive samples (metals) and currently is predominantly used in alloy analysis. The sample itself acts as the cathode, and an anode is brought very near to the surface. An electrical discharge is formed between the electrode and the sample and ablates some material while simultaneously creating a plasma. The ablated material from the sample is vaporized, atomized, and electronically excited in the plasma. Elemental components of the sample are identified by the presence of their persistent emission lines. This detection is performed either immediately after the plasma is created or after a delay to enable plasma cooling, and spectral simplification, to take place. The history of spark spectroscopy has been ongoing for 150 years, and innumerable journal articles, review articles and books have been devoted to the topic. A very small fraction of this literature is referred to in references [1–5].

Laser-induced breakdown spectroscopy (LIBS) is the topic of this book and requires no elaboration here; it suffices to say that it is a technique that is very similar to spark spectroscopy, except the spark is generated with an optically induced breakdown. The

Laser-Induced Breakdown Spectroscopy: Fundamentals and Applications, ed. Andrzej W. Miziolek, Vincenzo Palleschi and Israel Schechter. Published by Cambridge University Press.

energy for spark initiation can therefore be delivered remotely to the surface or volume to be analyzed. LIBS can be used to analyze both conducting and insulating materials.

We are developing SIBS as a simple, low-cost alternative to LIBS. One of the advantages of LIBS is the ability to easily process and analyze non-conductive material, and SIBS has a similar capability because the spark is generated between two rod electrodes. Material residing between the active electrodes is incorporated into the spark-produced plasma, and can therefore be analyzed. As with LIBS, the plasma is pulsed, and detection is delayed until the plasma has expanded and cooled and a significant amount of recombination has taken place. The efficiency with which the material to be sampled is taken into the spark is a function of the characteristics of the material. Various strategies are being used to make the SIBS output quantitative for different types of samples.

SIBS development at Physical Sciences Inc. (PSI) originally focused on measuring lead in airborne particulate material, specifically microparticulates in indoor rifle ranges. Inhaling this material is known to be harmful, and the current analytical methods cannot protect personnel in real-time. With a simple power supply and a detection system composed of interference filters and miniaturized PMTs, we were able to measure lead in real-time with a detection limit of 10 $\mu g\ m^{-3}$. Since that time, we have expanded the application of SIBS to measuring other airborne metals in real-time, developing a prototype field-screening monitor for trace metals in soil (with detection limits of about 20 $mg\ kg^{-1}$ for Pb, Cr, Ba, and Hg) and monitoring major components in cement. This wide range of applications demonstrates the utility and versatility of SIBS. Future developments will involve process control, both of particles entrained in gas flow and of solid materials, and other environmental applications, especially water analysis.

In the following three sections we present details of our SIBS development. Section 18.2 discusses the basic components common to all SIBS systems. Section 18.3 goes into more detail about the implementation specifics for two different applications, aerosols monitoring and soils monitoring. Finally Section 18.4 presents results from our investigations related to each of the aforementioned applications.

18.2 Basic description of SIBS processes and hardware

This section focuses on basic hardware used to apply SIBS to a variety of measurement scenarios. The first subsection focuses on the production of the SIBS spark; the second discusses detection strategies. The following section addresses details for implementation-specific elemental analysis of airborne particulate and of soil.

18.2.1 Spark characteristics

The heart of the SIBS apparatus is the spark-generating system, which consists of a pulsed high-voltage power supply connected to a closely spaced pair of electrodes. A high-voltage pulse applied to the electrodes causes the air between them to break down with the resultant production of a high-temperature plasma (we have calculated Boltzmann temperatures from iron lines as high as 20 000 K). Sample material in this plasma is vaporized and ionized. As

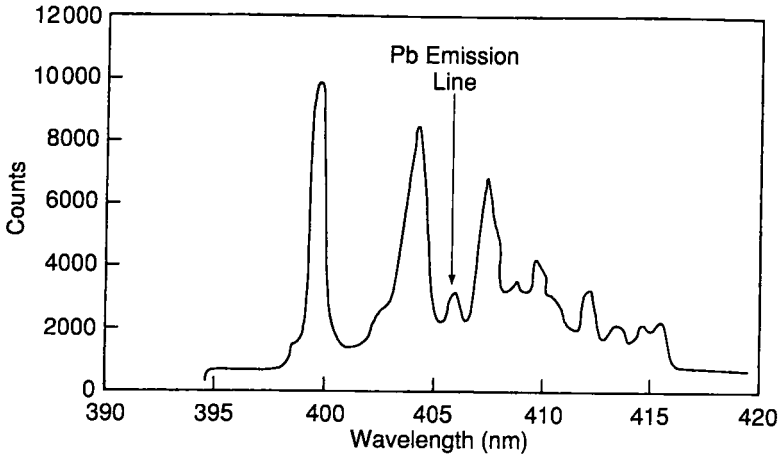

Figure 18.1. SIBS spectrum of Pb aerosol with no delay between spark and detection.

is the case with LIBS, the radiation arising from the SIBS plasma is analyzed to identify the species present.

The spark power supply integrates a standard pulsed, high-voltage supply (<2000 V, 100 J s^{-1}) with a capacitor bank. After the capacitors are charged, a trigger pulse initiates the creation of an ion channel between the electrodes through a high-voltage (15–40 kV), low-current pulse provided by a transformer. The threshold for this event is about 2.5 GW cm^{-1}. The ion channel creates a low-resistance path for the prompt discharge of the capacitor bank. The total discharge energy can be varied from 1 J to 5 J with <0.5 J arising from the initiator pulse. The spark repetition rate varies from a single pulse to about 10 Hz, the upper limit being determined by the power supply. Because of the large amount of current involved with the discharge of the capacitor bank (~ 500 A), the SIBS process can be considered a high-voltage breakdown followed by a classic arc discharge.

The spark occurs between two separated electrodes (typical gap is 5–6 mm) placed in or near the sample matrix. The electrode gap currently employed is the largest that enables reproducible spark formation. The electrodes are composed of proprietary materials, which have been chosen for high corrosion resistance, high melting temperature and low ablation propensity. Additionally, the electrode materials are unlikely analytes. In most cases, the electrode material does not add spectral complexity to the analyte signals.

The spark formed in SIBS has a visible volume on the order of 0.07 cm^3. This is considerably larger than a typical LIBS plasma (Radziemski and Cremers [6] report the spark volume from a 100 mJ Nd:YAG laser to be 0.003 cm^3). The greater sampling volume has some advantages, one of which is a greater likelihood of processing particles during each plasma event when measuring metals in airborne particulate material. Another advantage is that the amount of averaging necessary to achieve acceptable reproducibility often can be reduced, thus shortening analysis time.

The character of the light emitted in the breakdown region depends upon the delay after spark ignition. At times immediately after ignition (a few microseconds), the radiation is a spectral continuum characteristic of the emission of hot free electrons in the presence of

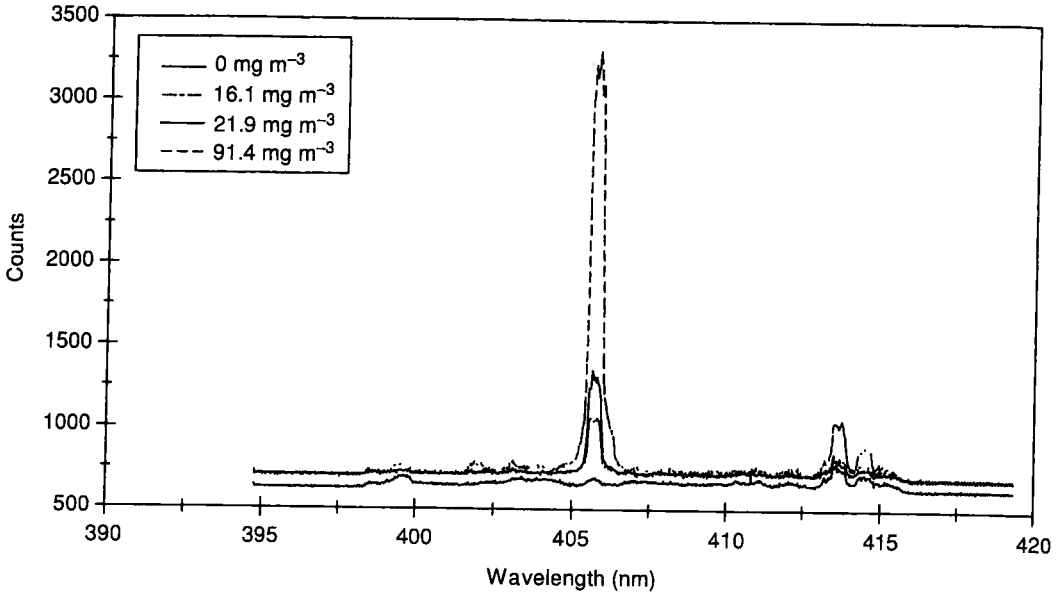

Figure 18.2. SIBS spectra in the region of 406 nm at different Pb-aerosol concentrations with detection delayed 75 μs after the excitation spark.

positive ions (Bremsstrahlung radiation), with little additional spectral structure, as shown in Figure 18.1. As the plasma cools, structured emission, characteristic of the species with high internal energy, principally ionized atoms, becomes more prominent. Continued cooling results in recombination of the ions with electrons and produces species of lower energy, which then emit light at their own characteristic wavelengths. As a result, the spectra become less complex at long times (>20 μs) after ignition, as shown in Figure 18.2. Typical delay times between 20 and 200 μs reject the bright continuum radiation due to plasma recombination and allow ready detection of the persistent atomic emission from the analyte metals. As in LIBS, the optimal detection delay is a function of power input: the higher the input power, the longer the optimal delay. Additionally, the optimal delay depends upon the element itself. For example, we have observed that sodium allows a longer delay for optimal detection sensitivity than does iron.

18.2.2 Detection systems

Analyzing the SIBS-produced plasma involves monitoring light emission intensities at a few selected wavelengths. Depending on the nature of the sample, the detection system is based on one or the other of two distinct strategies. The first, appropriate for spectral surveys to identify bright lines, as well as to analyze metals in complicated matrices, uses wavelength-dispersive spectroscopy. Here we use a grating spectrograph for the dispersion element. This approach is necessary in the analysis of soil, where iron is relatively abundant. Iron has a large number of lower-lying excited states that emit in the region where the features of the analytes of interest are normally found (300–450 nm). The ability to resolve spectrally the analyte features from iron lines is critical, since it is a dominant element in soils. Sometimes other elements also interfere with the analysis, but iron is the most common interferent.

In less complicated matrices, such as air, a combination of narrow-band interference filters and miniaturized photomultiplier tubes (PMTs) is used to detect the optical signals. The conditions under which this approach is used are very carefully screened beforehand with the wavelength-dispersive technique described above. In these studies, all likely interfering elements are added to the sample stream in quantities about 1000× their normal abundance. If, in this situation, there are no observed spectroscopic interferences, the PMT approach is deemed acceptable.

The wavelength-dispersive detection system consists of a lens to collect light generated in the spark region, an optical fiber to transmit the light to the entrance slit of a spectrometer, and an intensified linear photodiode array at the exit plane of the spectrometer (the spectrometer/photodiode array configuration is known as an optical multichannel analyzer or OMA). For most of these studies, we have used a spectrometer having a 0.32 m focal length and a 2400 g mm^{-1} grating. This system has a spectral dispersion varying from about 0.03 nm $pixel^{-1}$ at 250 nm to about 0.02 nm $pixel^{-1}$ at 600 nm. The overall spectral resolution, defined as the full-width at half-maximum of an isolated atomic line, varied from about 0.15 nm in the ultraviolet to about 0.10 nm in the visible. For wavelengths longer than 450 nm, a 420 nm cut-on glass filter is placed in front of the monochromator slit to remove second-order spectral features.

As mentioned above, the fluorescence detection relies upon a timing system that delays the detection of the atomic emission a suitable time after spark initiation to eliminate interference from the prompt spark-plasma emission. Our spark-generating power supply is driven by a delay generator that allows the sparks to occur at set intervals. Spark events trigger the detection system by activating a second delay generator. This generator delays the turn-on time of the OMA, so that the OMA will not be saturated by the very bright early plasma of the spark. The OMA is then kept activated for a set time (gate time) and detects emission from the cooling plasma.

By carefully choosing appropriate delay and gate times, we can optimize detection conditions for a given element. Generally, longer delay times are beneficial because, even though total intensity is reduced, the signal-to-noise ratio is better. As mentioned, typical delay times vary between 20 and 200 μs. Typical gate times are 10–50 μs. The OMA can be set to accumulate signal from a series of sparks or, as is often the case, the light from a single spark provides sufficient signal for a complete spectrum.

In the case of a relatively simple matrix, optical signals are collected radiometrically with a pair of filtered, miniature photomultiplier tubes. The delay time is typically 20–50 μs with an equivalent integration (gate) time. The advantages of the filter and PMT approach include simplicity and low cost. The strategy behind the radiometer is to accumulate the signal associated with the atomic line (on-line) with one filter and to subtract any background signal with a nearby filter (off-line) that has no analyte or electrode atomic features inside its bandwidth. For lead, the Pb(I) line at 405.8 nm is used with 400 nm for background. For chromium the Cr(I) line at 427.5 nm is used with 420 nm for background. The filters have pass-bands of 1 nm FWHM (full-width, half-maximum). Figure 18.3 shows the transmission curves of the on-line and off-line filters for lead analysis superimposed over a wavelength-dispersive spectrum taken of lead aerosol.

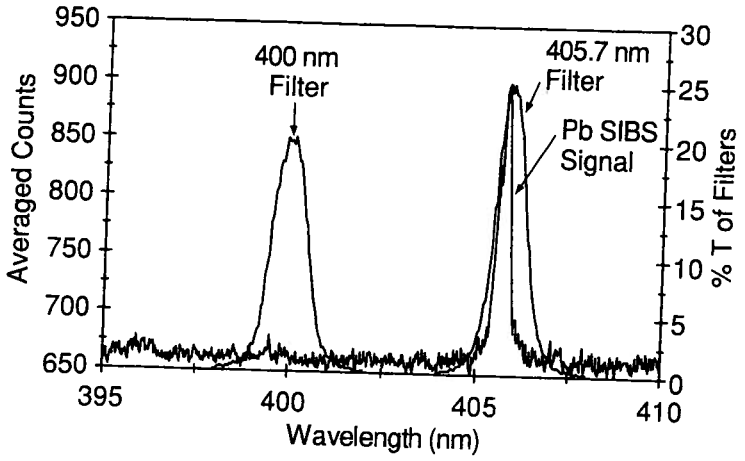

Figure 18.3. Transmission curves of interference filters superimposed on aerosol lead spectrum.

18.3 Application-specific considerations

18.3.1 Aerosol metals monitoring

Metals in airborne particulate are a recognized respiratory health hazard in many venues, especially in factory workplaces. Most monitoring of these materials is now performed with a relatively long-term filter collection period followed by laboratory analysis of species captured on the filter. Currently, there is no widespread method to monitor the hazardous components of airborne particles, and therefore no way to protect human respiratory health in real-time.

Aerosol monitoring hardware and analytical methods

Aerosol monitoring is accomplished by pumping contaminant-laden air through the spark gap at a known rate with a pump. Fiber optic cables transmit the optical emission from the spark-induced plasma to the detection system. Figure 18.4 shows a diagram of this apparatus.

Airborne particulate usually provides a relatively simple matrix and the PMT/interference filter approach is sufficient. The PMTs supply output voltages that are proportional to the amount of light in the pass-band of the interference filter. These analog signals are input into a 1.2 MHz A/D data acquisition board incorporated into a PC (100 MHz Pentium). The temporal traces of the PMT signals are analyzed using custom routines developed with Lab Windows CVI software [7]. The on-line and off-line temporal traces are subtracted and the difference is then integrated. This difference signal is then compared with a previously acquired calibration curve (see below) and presented in strip-chart fashion as concentration versus time. In most cases, the data are averaged and reported at 2 min intervals.

Recently, we have packaged the components of this breadboard into a single unit, as shown in Figure 18.5. The air to be sampled can be drawn though an optional cyclone, to eliminate non-respirable particles if desired, prior to flowing through the spark chamber.

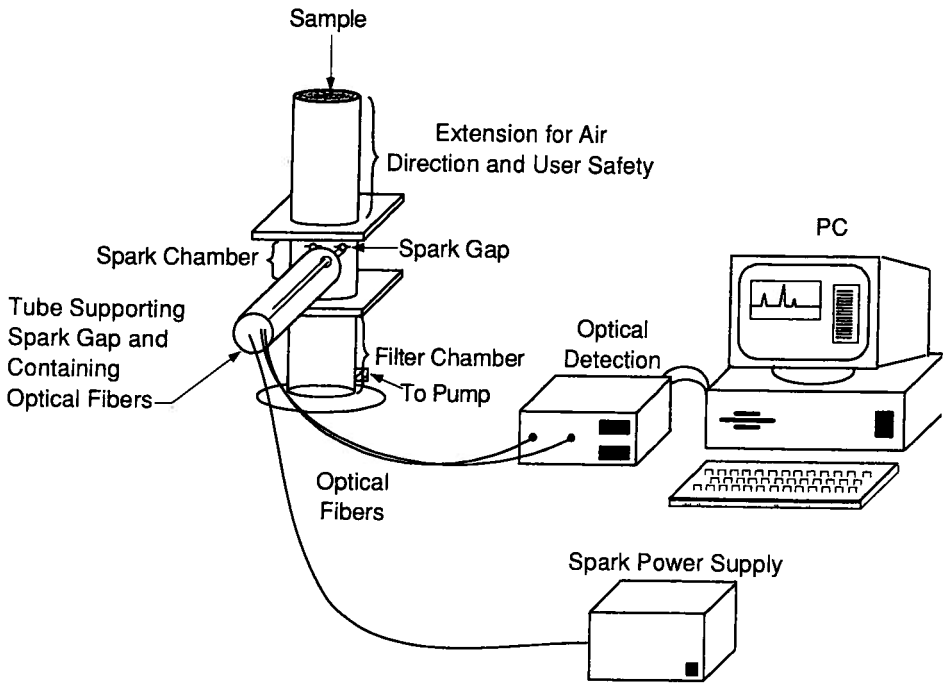

Figure 18.4. Diagram of laboratory breadboard SIBS monitor for lead in airborne particulate.

The air then passes through a filter, which is used to collect a sample for laboratory analysis and correlation, and exhausted out the rear of the unit. The sub-unit containing the sampling cell can be separated from the data acquisition sub-unit for monitoring in hazardous environments. In this situation, the sampling unit can be placed in the environment being monitored, and the user and data acquisition unit can safely operate from a remote location.

Dry aerosol calibration system

To calibrate the instrument for dry metal-laden aerosols we devised a system to produce well-characterized flows of dry aerosols. The method involves injecting droplets of known size and formation rate made from a solution of known metal concentration into the top of a drying column. As the droplets traverse the column, all water is evaporated, leaving solid particles of known size and concentration. We have used two different droplet generators in our work. The first of these was based on the design demonstrated by Berglund and Liu [7]. Similar systems have been employed by other researchers; see, for example, the work of Zynger and Crouch [8]. The operating principle involves the imposition of a periodic instability on a thin stream of fluid flowing through a pinhole orifice. The instability is induced by coupling a high-frequency vibration into the fluid using a piezoelectric transducer driven by a square wave function generator. Under certain conditions of fluid flow rate and instability frequency, monodisperse aerosols are generated. For our usual operating conditions, this system produced droplets 48 μm in diameter.

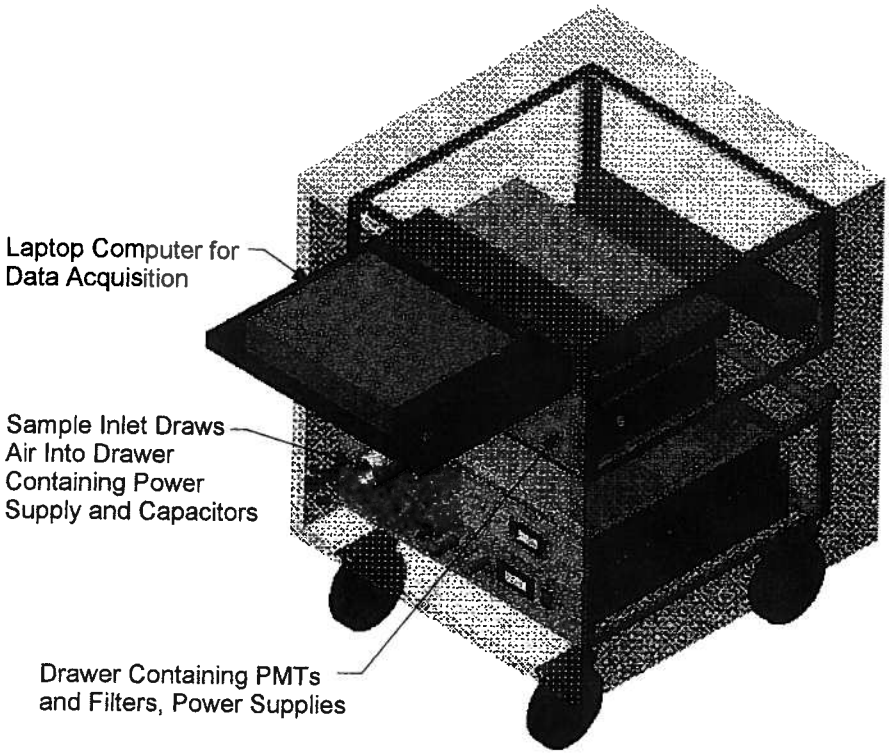

Figure 18.5. Diagram of alpha-prototype SIBS monitor for lead in airborne particulate. This instrument was designed for application to workplace hygiene measurements.

The second droplet generator is a commercial atomizer nozzle (Sonotek). The Sonotek unit generates polydisperse droplets ultrasonically with a narrow distribution centered at 18 μm in diameter. It is much the easier of the two to operate, and the non-monodisperse character of the output does not affect the SIBS signals. This is primarily because of the large number of particles produced by the generator. It produces an output stream of 2.4×10^5 particles per second, so many particles (40–50) are processed by each spark.

The droplet generator is situated at the top of a Plexiglas tube in a downward-directed orientation toward the drying column (Figure 18.6). Air is drawn at a fixed rate through a porous, stainless steel inner sleeve in order to minimize loss of particles on the drying column walls. The flow rate (0.028 m^3 min^{-1}) exceeds the particle terminal velocities. The air is heated to 110 °C to evaporate solvent (water) from the droplets and is drawn out the bottom of the column by a filtered pumping system. The dry aerosol (0.1–3 μm diameter) is trapped on a filter placed at the bottom of a Plexiglas extension under the drying column that houses the spark chamber. This filter prevents particles from exiting the generator and contaminating the air pump. We have verified gravimetrically that 80%–95% of the dry mass exiting the droplet generator passes through the spark region to be collected by the filter.

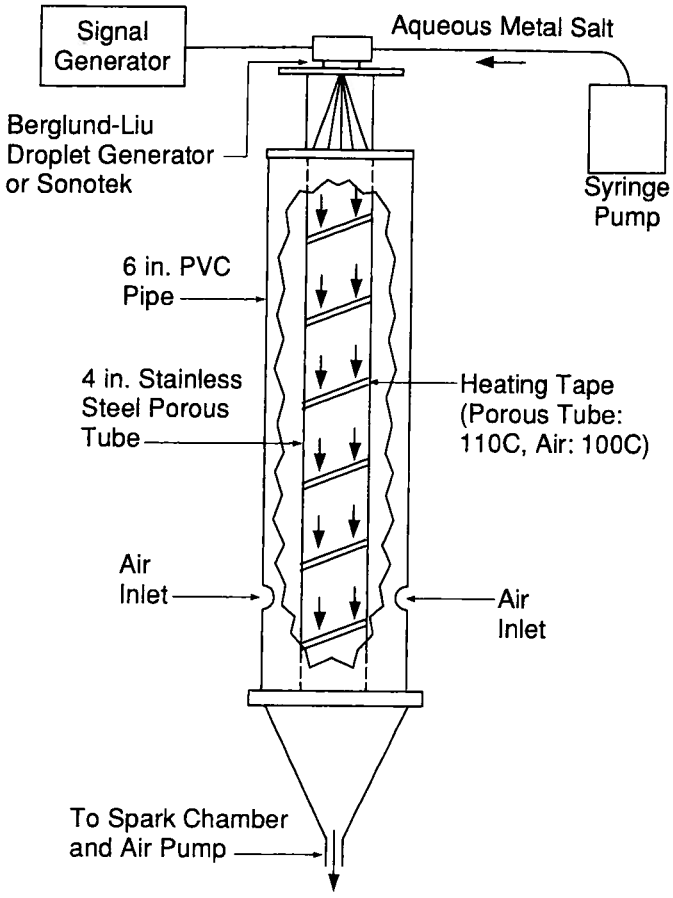

Figure 18.6. Dry aerosol generator with Berglund–Liu droplet generator.

Speciation, particle size and realistic samples in aerosol measurements

We have studied the possible effects of speciation on the airborne particulate signal in a variety of ways. Possible changes in signal level between various metal salts were easily studied with the previously described aerosol generator using dry aerosols of identical concentrations (440 $\mu g\ m^{-3}$) of lead chloride, nitrate and acetate. These aerosol concentrations were sampled one after another, allowing the signal to return to near baseline between additions. The resulting data showed no detectable distinction between the three types of lead species. Similar assays were performed with a variety of water-soluble chromium compounds.

Actual airborne analysis will, however, not likely involve water-soluble metal salt particles. Instead, these measurements will involve elemental and oxide particulate. It is more challenging to look for this type of speciation effect, since these compounds are not water-soluble and test particles cannot be generated with the dry aerosol generator previously described. For these tests, other methods of particle generation have had to be used. The SIBS signals obtained for these aerosols were time averaged and compared with correlative filter samples analyzed for total metal content by an independent laboratory.

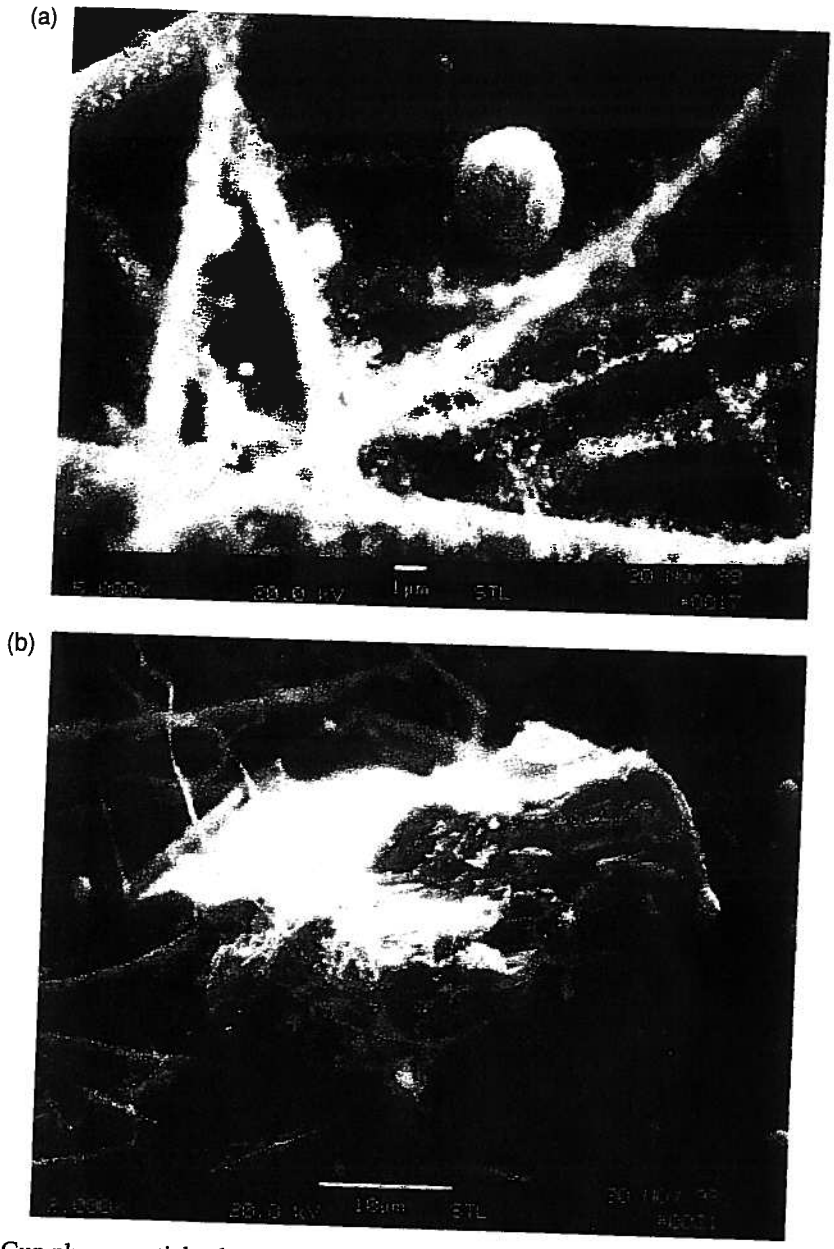

Figure 18.7. Gun plume particle elemental analysis – SEM photomicrographs showing (a) small and medium size particles and (b) a large particle. The larger particles are probably spalled bullet material remaining in the muzzle, the smaller ones created by combustion of the lead styphnate within the primer material.

The first of these test aerosols was generated by firing blanks from a handgun (Smith and Wesson 357 Magnum) in the laboratory. We drew samples of the plume from several shots through the SIBS system and subsequently trapped the particles on an internal filter. The particles trapped on the internal filter were submitted to an independent analytical laboratory for scanning electron microscopy (SEM) and energy-dispersive X-ray analysis

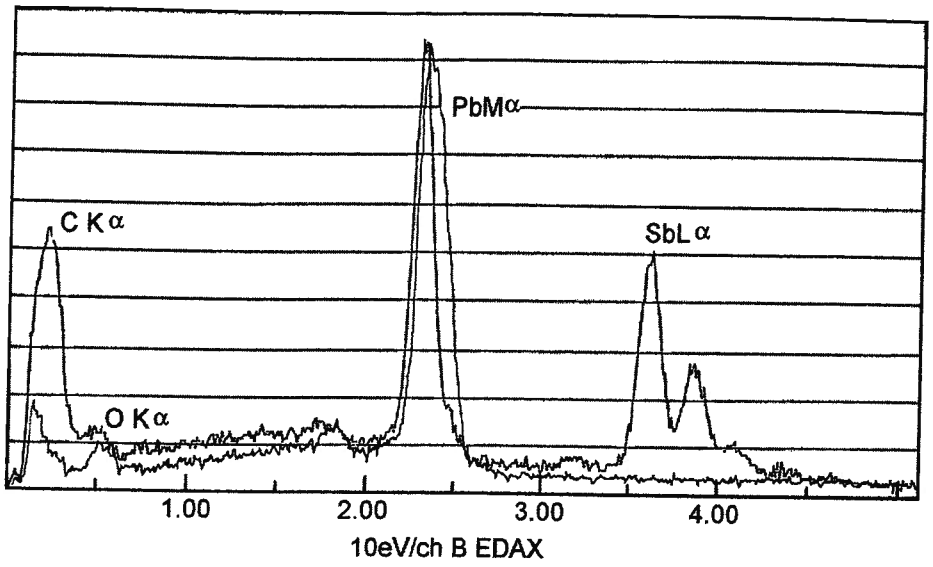

Figure 18.8. EDAX analysis of particles obtained by firing blanks from a handgun.

(EDAX) analysis to verify the presence of lead and lead oxide (Figures 18.7 and 18.8) and to quantify the total amount of lead collected. The SIBS lead mass was obtained by temporally integrating the data and convolving the air-sampling rate (1.3 cfm). The correlative data were obtained by acid digestion of the internal filters and subsequent ICP analysis of the digestate.

The integrated signal from the SIBS monitor was consistent with the total lead mass measured from the internal filters. The results showed 140 μg of lead collected on the filter compared with 144 μg determined by the SIBS monitor. A second comparison produced 69 μg of lead on the filter versus 100 μg predicted. This shows that the SIBS monitor responds to lead oxide similarly to other lead compounds. More thorough verification of the ability of the SIBS monitor to measure lead in elemental and oxide forms is currently under way.

The SEM analysis shown in Figures 18.7a and 18.7b also indicates at least three classes of particle size fractions, one at 50–100 nm in diameter, another at 0.5–3 μm and a third at 15–45 μm diameter. The largest are likely the result of residual spalled lead material in the gun barrel. From the SEM photographs, we estimate that the first two mass fractions account for the majority of the mass. Our initial analysis indicates that SIBS is accurately responding to these size lead/lead oxide particles (up to at least a few micrometers). The EDAX analysis (Figure 18.8) shows the presence not only of lead, but of oxygen, indicating the presence of at least an oxide layer on these particles. Also observed were antimony features (from the lead styphnate primer) and carbon (from filter material).

To further test the ability of SIBS to analyze realistic samples, we prepared an aqueous solution of lead nitrate and a small mass of coal ash. The ash used in this test had a median particle diameter of 0.5 μm and was composed mostly of iron, aluminum, and silicon oxide. This mixture readily passed through the ultrasonic aerosol generator to produce individual

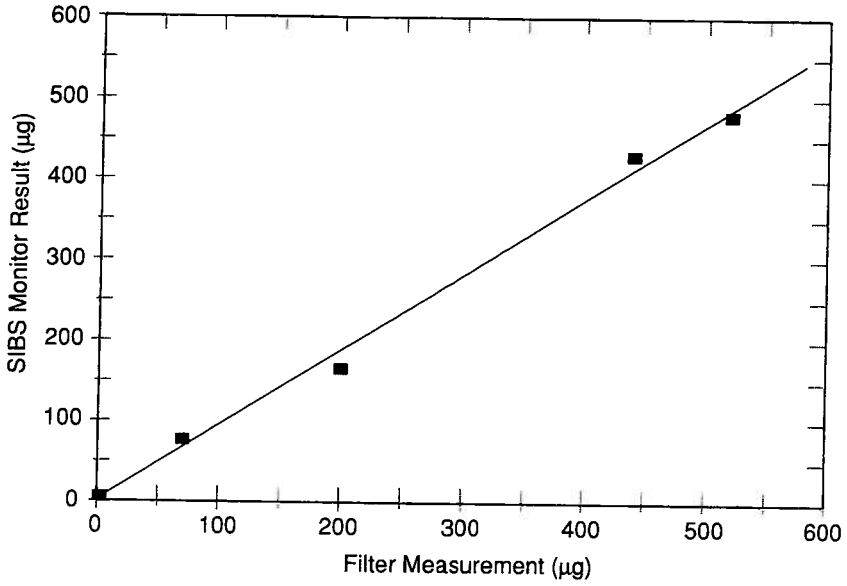

Figure 18.9. Integrated signal from the SIBS monitor versus total chromium mass measured from the internal filters. Good correlation between the two implies that SIBS monitoring of chromium is free from speciation effects, and also that real-time SIBS measurements could replace the filter-based ones.

and agglomerated ash particles containing condensed lead nitrate such that the final predicted lead concentration in air was 120 $\mu g\ m^{-3}$. The SIBS monitor produced the lead response predicted from our calibration curve (made with dilute solutions of lead nitrate) indicating that these particles, which are principally composed of aluminum, silicon, and iron oxides, are being vaporized and excited in the SIBS spark.

We also addressed the problem of chromium speciation and have determined that SIBS exhibits equivalent response to two chromium valences (Cr(III) and Cr(VI)). We used SIBS to measure chromium above a hard chromium plating tank and compared our results with those from filter samples of mixed Cr(III) and Cr(VI) oxides. Figure 18.9 shows the excellent correlation between the SIBS and filter results. The filter analysis is based on OSHA draft method ID-215, a filter digestion followed by ICP analysis [9]. The detection limit associated with this analysis is about 5 $\mu g\ m^{-3}$. This detection limit is similar to those usually reported in LIBS analyses. There have been optimized LIBS systems that are capable of monitoring airborne chromium down to 0.4 $\mu g\ m^{-3}$, but the hardware needed is more complex than that described here. Note also that the SIBS results are available in real-time, unlike those from the filter analysis.

Interference measurements

The primary interference in SIBS is spectral overlap of analyte emission lines with emission from other species present in the sample. This is an especially important issue in the case of the airborne metals monitors, because for the most part, signal acquisition is performed by narrow bandwidth interference filters and miniature photomultipliers. The 405.7 nm Pb atomic line and 400 nm off-line wavelengths were initially chosen because they were

suitably free from electrode lines. To verify that these lines are free from interference by other species likely to be present in a real-world sample, we prepared solutions of iron, aluminum, silicon, calcium, and magnesium such that $>1000\ \mu g\ m^{-3}$ concentrations would result in the aerosol generator.

Spectrally resolved data were then taken with a Princeton Instruments optical multichannel analyzer/monochromator combination. The results indicated there to be no spectral interferences from these elements in these wavelength regions at the bandwidth (1 nm FWHM) of the radiometer filters. Similar tests have been conducted with lead paint samples where the following atomic lines in the 392–418 nm region are observed: Al(I) – 394.4 and 396.15 nm; Mn(I) – 403.31, 403.45, 404.51, and 406.35 nm; Fe(I) – 404.58 and 406.36 nm; Pb(I) – 405.78 nm. None of these features falls within the spectral bandwidth (1 nm FWHM) of the lead feature and so they are not expected to provide a spectral interference in the SIBS sampling. This is particularly important for airborne monitoring of lead paint abatement. We have also taken similar data for lead paint that show prompt Ti lines in this region from this paint component. Proper choice of delay time readily discriminates against these features. Additionally, they do not spectrally overlap the Pb line.

18.3.2 Metals monitoring in soil

In general, disposition and/or treatment of contaminated soil is controlled under TCLP (toxicity characteristic leaching protocol, found in 40CFR 266 Appendix VII) limits [10]. TCLP is a process where the soil is gathered (either from the surface or from core samples) and submitted to a laboratory leaching procedure. This procedure, performed with weak acids, has been developed to imitate long-term leaching conditions in a landfill, and regulations written around the possibility of ground-water contamination. Because the material is diluted 20 × in solution during this test, if the amount of total metal in the sample is less than 20 × the TCLP limit it cannot fail to meet the regulations. For this reason, 20 × TCLP is our sensitivity goal for each metal in soil.

Despite the desire of the remediation community, there are no widely used field-screening methods for the on-site determination of metals in soil. There are two EPA-approved field-screening methods for metals in soil, a general method for portable X-ray fluorescence analyzer use [11] and an antibody-based method for mercury, but these methods are of limited value to most remediation efforts [12]. While the XRF analyzer is sensitive enough for some elements (Pb), it is inadequate for detecting others (Cr, Hg, etc.) [13]. We have started to develop a SIBS-based soil monitoring method which should work for a larger number of contaminant species.

Soil monitoring hardware and analytical methods

With airborne particle analysis, samples are positioned and refreshed by drawing air through the electrode gap with an air pump. Solid samples require a different approach. In our initial investigations, small quantities of the loose samples are placed on a Plexiglas sheet. The electrode assembly (see Figure 18.10) is then placed over the sample. In most cases, one of the electrodes is in direct contact with the soil sample. The spark process creates a

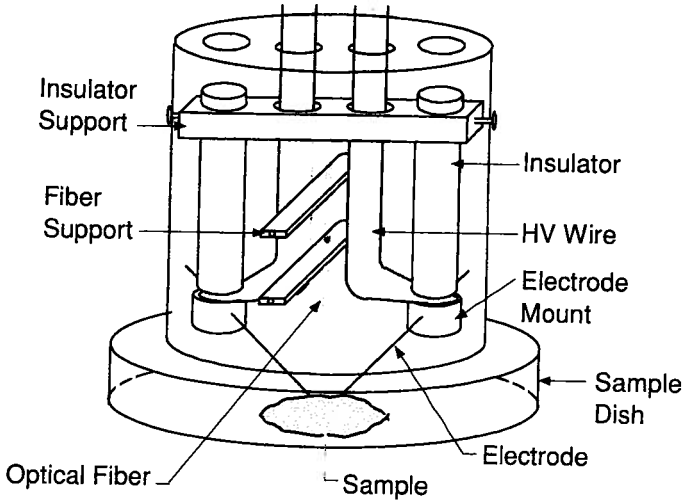

Figure 18.10. Diagram of SIBS soil analysis sampling interface.

shock wave that lifts some of the sample into the spark region where it is subsequently vaporized and excited to emitting electronic states. The shock waves can also disperse some of the sample, so the electrodes are repositioned, as needed, between sparks to ensure they remained in close proximity to the sample. The basic procedure has been to take 10 successive spectra, each one consisting of light collected from two successive sparks, and then to average the 10 spectra together. We generally acquire three such sets of spectra for each sample. The whole measurement process takes 2–3 min.

The electrodes are cleaned between samples by first swabbing them with a dilute solution of nitric acid, rinsing with deionized water, and finishing by swabbing with methanol. Then the system is allowed to spark in air for a minute or so before a new sample is poured out onto the Plexiglas sheet. This procedure guards against results being biased by material adhering to the electrodes from previous samples. The efficacy of this approach is proven; there is no effect of analysis order on signal level.

SIBS can be used to quantify metals in soils using standard addition analysis. This is a well-developed and accepted method in analytical chemistry in which known quantities of the analyte of interest are added to weighed sub-samples. These sub-samples are then analyzed. Extrapolation of the signal versus "added concentration" line to the y-axis yields the signal associated with the unknown. Dividing the y-axis intercept by the slope of the line yields the concentration of the unknown.

This method is important in quantitation because it allows the effects of the matrix to be removed from the analysis. Because soils are a widely varying and inhomogeneous matrix, standard addition analysis allows SIBS to be applied to different types of soil in a way that a single calibration curve cannot. Practically, this will not be onerous in fieldwork, because at each site there will usually be only a few types of soil present. In these cases, then, it will be possible to construct a standard addition plot for each soil type, and then use that plot as a calibration curve for other samples having the same physical and chemical characteristics. In our research, size of the sub-samples is usually about 1 g, but this can be varied with the textural scale of the soil.

Because no effort is currently made to control the amount of material processed with each discharge, there is considerable variation in intensity between spectra taken during a sample run and even between the 10-spectrum averages from each run at a given concentration. As a result, a meaningful standard addition curve cannot, in general, be made by plotting just the absolute intensity of the analyte lines for each sample at each concentration. There is, however, good linear correlation between the ratio of the intensity of the analyte features to one of several nearby iron lines, which are also excited in the spark plasma, and the concentration of metal in the sample. The reason for the normalization procedure is that differences in the line intensities between spark events are indicative of differences in the strength of the spark excitation itself and also in the amount of material present in the spark region during the analysis. The iron content of the soil sample does not vary with the amount of analyte in it as standard addition is applied (although, of course, it would be different for soils taken from different geographical locations), so provides a useful marker for both the strength of excitation of the sample and the amount of material in the spark region.

Spectral surveys to find optimum lines for analysis

There are a number of potential lines one could use for analysis of soil for metals content. Three important criteria in choosing an appropriate line for further investigation include the intensity of the line itself, whether it be free from interference by lines from other elements in the soil, and whether there be nearby lines from iron, or some other relatively abundant and constant component of soil. These lines can be used to normalize the contaminant spectral intensities so as to compensate for variations in spark strength and in amount of material in the spark region. The order of these priorities changes with characteristics of the analyte atom. The more toxic and tightly regulated the target analyte, the more sensitive must be the measurement. Therefore, in the case of mercury, finding a sensitive line is important (for example in order to pass TCLP, total mercury in soil must be <4 mg kg^{-1}). In other cases, emission lines of the analyte are bright, but the material is regulated at a much higher level. An example of this situation is the measurement of barium (which has a $20 \times$ TCLP limit of 2000 mg kg^{-1}).

The line intensities in the averaged spectra are calculated as peak heights from a local baseline. The local baselines for each spectral feature are calculated as an average of the local minima on either side of the line. This procedure is more essential for cases where there is some partial overlap with bright adjacent lines or when the background continuum radiation is non-uniform. This more detailed spectral analysis improves the overall data quality considerably compared with using a peak height above a common baseline, because of reduced scatter between replicate sets of data.

18.4 Applications and results

In order to demonstrate the versatility of SIBS, we present two applications: (a) the measurement of lead in airborne particulate, and (b) the analysis of soil for trace metals.

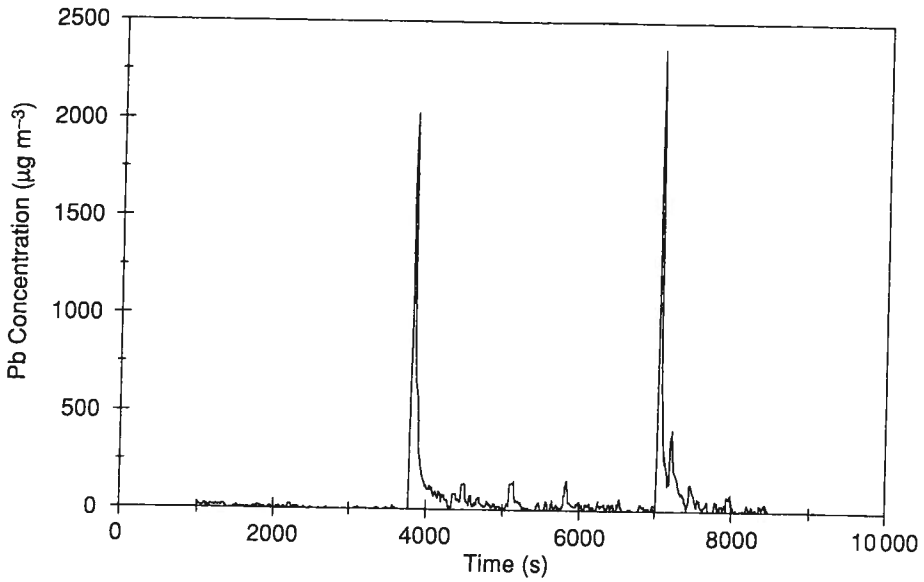

Figure 18.11. Lead signal versus time from firing range data, at location of shooters.

18.4.1 Lead in airborne particulate application: firing range tests

We performed two field tests of the airborne lead monitor at a nearby firing range. The range is a sophisticated facility with a filtered recirculating ventilation system. The airflow entrains the lead and carries it away from the shooters downrange through the ventilation system and into a set of HEPA filters. For the first test the lead monitor was positioned immediately in front of one of the 20 firing booths. Active handgun firing was occurring at a booth 10 ft to the right of the test position. During these tests 15 booths (shooter locations) were active.

Quantitative data acquired during this test are shown in Figure 18.11. The vast majority of the data show the measured lead concentration to be at or near our detection limit of 10 $\mu g\ m^{-3}$, well below the OSHA regulated level of 50 $\mu g\ m^{-3}$. A few events recorded lead concentrations exceeding 100 $\mu g\ m^{-3}$. The events showing lead concentrations above the detection limit involved a shooter discharging firearms directly above the sample inlet (vertical distance < 1 ft). The first of these occurred near 3900 s when four revolver rounds were fired in quick succession. The second event near 5900 s occurred when two full magazines from a semiautomatic pistol were fired, again directly over the sampling inlet of the instrument. Finally, in the time 7000–7300 s two different weapons were fired. It may be that in these cases the instrument is measuring larger particles as they settle into the sample inlet. Smaller particles (i.e., respirable ones) may still be pulled downrange by the air handling system.

In the time period 6000–7000 s we tested lead-free ammunition. No significant lead readings were obtained when this ammunition was discharged directly over our sample inlet. Additionally, at 5100 s approximately 12 individuals simultaneously fired two or

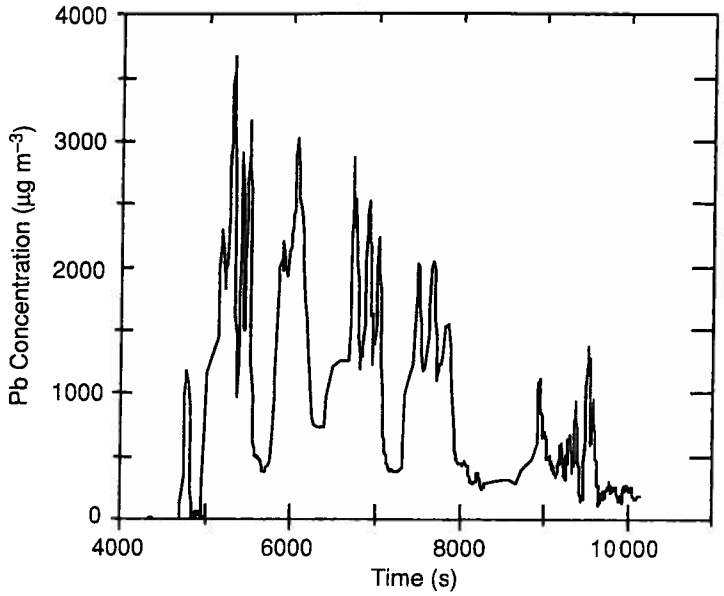

Figure 18.12. Lead signal versus time from firing range data, downrange directly before air filtration.

more clips consecutively. The signals appeared simultaneously with the smell of smoke at the sampling location.

This well-designed range is clean and free of lead contamination. Many other firing ranges, particularly those of older construction and in private use, often have transient airborne lead levels approaching 2000 μg m^{-3}. The time-weighted average (TWA) of lead data for the test period was 54.3 μg m^{-3}, which is above the regulated 50 μg m^{-3} limit. However, this is an extreme exposure upper limit as the majority of the data were deliberately introduced by firing above the instrument inlet and were not representative of the shooter's airspace. Even with this caveat, however, an 8 h TWA of the data works out to 13.5 μg m^{-3}, well below the action level because the shooting during the test period was the only range activity on that day.

A second test was also performed at this range. For this entry, the lead monitor was placed downrange in the ventilation crawlspace immediately before the contaminated air passed through the filters. The data are shown in Figure 18.12. We have excluded all of the data before 4000 s because this was before any firing occurred and there were no measurable lead signals.

Slightly before 5000 s the ventilation system was activated. The turbulent airflow agitated lead particulate in the ventilation room, producing the first visible lead signal in this data set.

When active firing took place the concentration reached as high as 3000 μg m^{-3} in the ventilation room. This is consistent with published values in firing ranges without active, filtered ventilation systems. This sophisticated range reaches this level only in the ventilation crawlspace just before the filters. The airborne lead and lead oxide are carried by the airflow

from the shooting positions to the HEPA filters, consistent with the data obtained with our SIBS monitor.

The data show four separate active periods of firing, each with spikes corresponding to different levels of activity. During the test we were able to correlate each of the enhanced lead concentration spikes with audible periods of firing. The inactive periods between shooting were not sufficiently long for the monitor signal to return to baseline values. This is probably representative of the clean-out time of the particles from the range airspace. Finally, at the end of the test we observed the lead produced from a single shooter.

The TWA exposure data for Figure 18.12 are 950 $\mu g\ m^{-3}$ for the test period and 178 $\mu g\ m^{-3}$ for 8 h. This latter value is well above the regulated limit and supports the decision of the range designer to provide access to the crawlspace only through a sealed panel.

18.4.2 Soil results

We present here the SIBS analysis of three different soil types for both lead and chromium. The three soils are Andover soil, i.e. soils taken outside our laboratory, and two NIST Standard Reference Material (SRM) soils, SRM 2709, or San Joaquin soil, and SRM 2710, or Montana soil. The SRM soils were certified to have specific levels of lead and chromium. We sent samples of the Andover soil to an outside laboratory (Chelmsford, MA) for analysis for independent verification of our results. We also did a limited number of tests using fine SiO_2 particles as a simulant for sand.

Initially, the Andover soil samples were tested in three forms: loose, compressed into pellets, and compressed with a binder compound. These forms were chosen because of their similarity to those used in the XRF analysis protocol. Loose samples were prepared by drying to remove residual water and manually separating out large stones. Drying is necessary to allow comparison between our method and other laboratory methods, which report metals content in dried samples. To prepare compressed pellets, small aliquots ($\sim$0.5 g) of soils were pressed in a hydraulic press to between 8 and 9 tons. The pellets so prepared were 13 mm in diameter and about 2 mm thick.

Compressing the soil with added binder (17% cellulose) improved the integrity of the pellets, but at a cost of greatly reduced signal levels. These pellets were quite hard, and the sparks ablated only very small amounts of material from them. Compared with loose soil sample signals, pelletizing the Andover soil resulted in reductions in signal levels by factors of 3 to 5 when no binder was used and by factors of 10 to 20 when binder was added. The reduced signal levels had the effect of increasing the uncertainty in our measurements substantially.

A typical spectrum of loose Andover soil is shown in Figure 18.13. The most prominent features in the spectrum are iron lines at 404.58, 406.36, and 407.17 nm, and a line at 407.77 nm which is a strontium line. The lead line appears at 405.78 nm.

As previously detailed, data analysis involved measuring the peak height of the feature of interest, subtracting a local baseline and normalizing the intensity to that of a nearby iron line. The relationships between intensity ratios and concentration of lead in the sample are

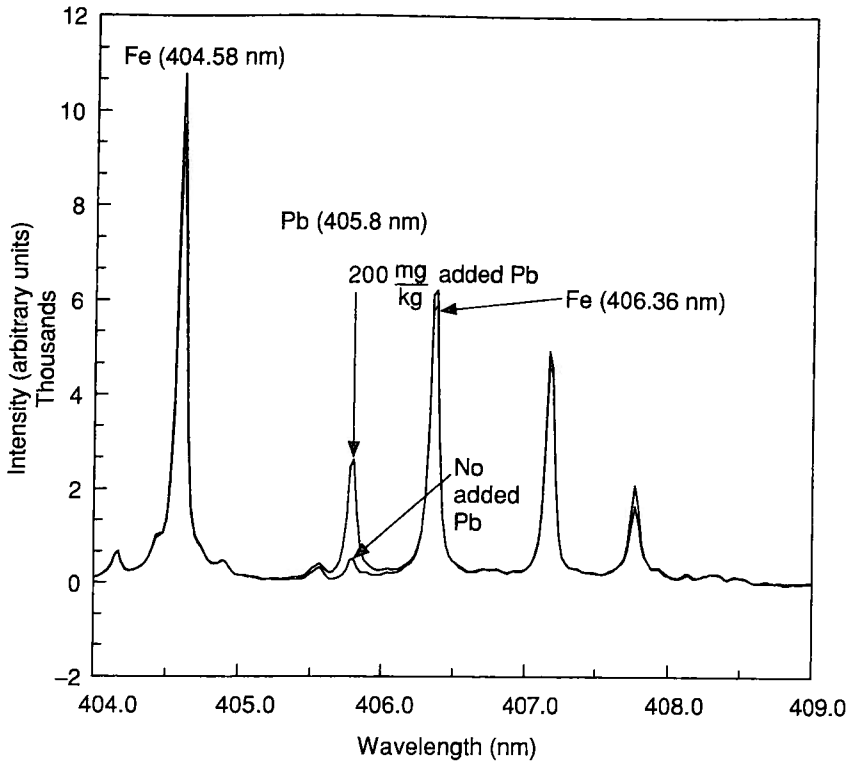

Figure 18.13. Spectra of Andover soil between 404 and 409 nm with and without added lead.

shown for the three samples in Figures 18.14–18.16 for loose soil, pelletized soil, and sand respectively. In Figure 18.14 the 404.58 nm iron line was used for normalization. In Figures 18.15 and 18.16 it was the 406.36 nm line. Derived sensitivities were the same regardless of which of the three iron lines was used for normalization (normalizing to the 405.17 nm line also gave results similar to those shown here). All plots were well behaved and linear.

When pelletized, the Andover soil had (Pb/Fe) ratios similar to the loose soils, but overall signal intensities were much lower. The net effect of this overall decrease in intensity was an increase in variability in the measurement and therefore an increase in the uncertainty in quantitation. The SIBS spark is largely a thermal event that happens near to the sample surface, as opposed to the LIBS process where energy is directly focused onto a surface for analysis. In the case of SIBS, shock waves can raise loose material into the thermal plasma, but have little effect in ablating material from the surfaces of compressed pellets. Thus, in the case of pellets, only a relatively small amount of material is removed into the plasma via thermal ablation induced when the outer edges of the plasma impinge on the pellet's surface. Despite the drop in overall intensity in the case of the pellets, it is important to note that the means of the signal from both the pelletized and loose samples overlay each other. The best-fit lines of both sample types coincide, but almost all of the raw data from the pelletized sample lie outside the $\pm 1\sigma$ range of the loose soil data. This increased variability is reflected in the higher detection limits associated with pelletized samples shown in Table 18.1.

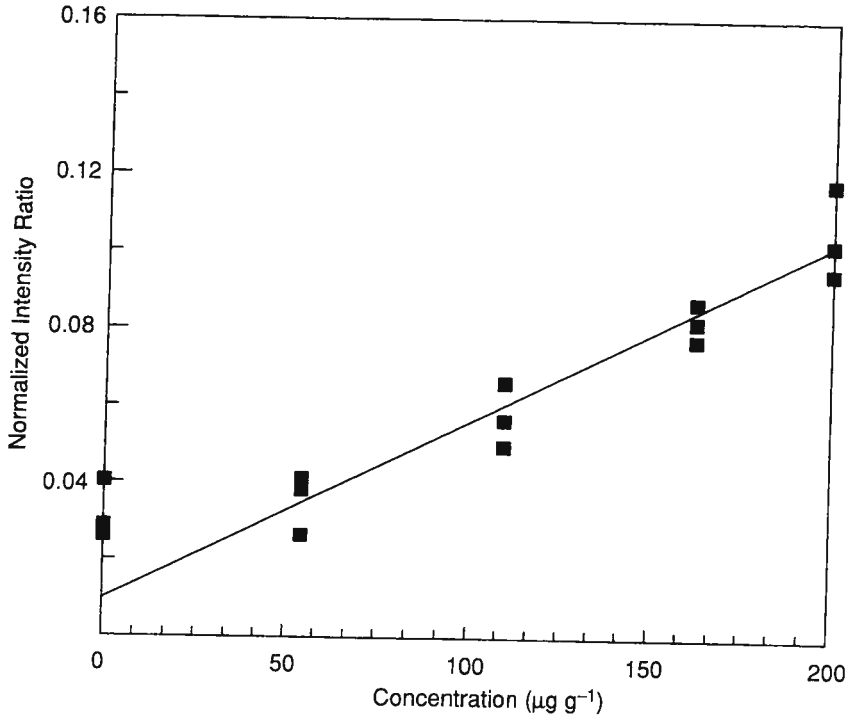

Figure 18.14. Ratio of the height of the lead feature at 405.78 nm to that of the iron line at 404.58 nm shown as function of added lead in the loose Andover soil sample.

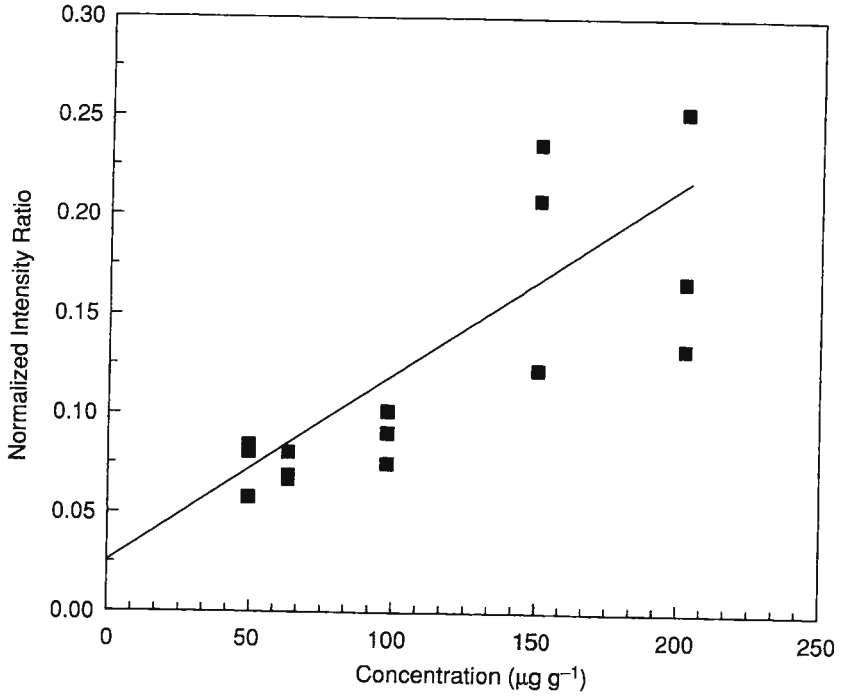

Figure 18.15. Ratio of the height of the lead feature at 405.78 nm to that of the iron line at 406.36 nm as a function of added lead in pelletized Andover soil.

Table 18.1. *Loose versus pelletized versus pelletized with binder SA results*

Preparation technique	Detection limits (1 σ)
Loose soil (dried)	<20 mg kg^{-1}
Pelletized (dried)	~30 mg kg^{-1}
Pelletized with binders (dried)	~70 mg kg^{-1}

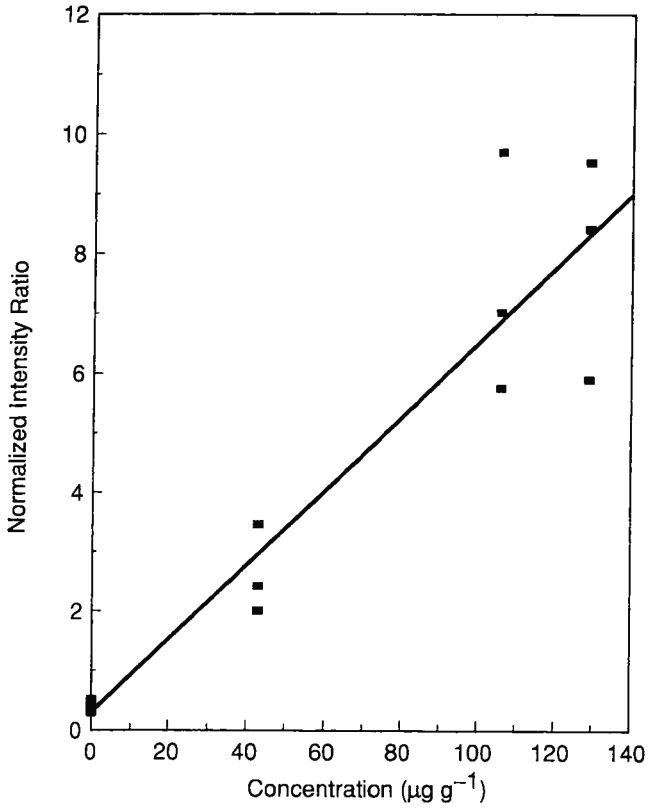

Figure 18.16. Ratio of the height of the lead feature at 405.78 nm to that of the iron line at 406.36 nm as a function of added lead in loose sand.

Samples were also prepared with added levels of 500 mg kg^{-1} and 1000 mg kg^{-1} of lead to examine calibration curve linearity at high levels of contamination. Figure 18.17 shows a standard addition curve combining data taken at lower levels with the results of soils spiked at higher levels. The curve is linear up to 500 mg kg^{-1} of added lead, but falls off at the highest concentration plotted. The intercept from this plot (fit through 500 mg of added Pb per kilogram of soil) gives results consistent with our data shown in Figure 18.14 as well as with out-of-house laboratory analysis, namely a natural level of lead in the soil of 33 $\pm$ 18 mg Pb per kilogram of soil. This rollover will probably not affect actual use of a field-screening monitor since it occurs at high lead concentrations ($\gg$100 mg kg^{-1},

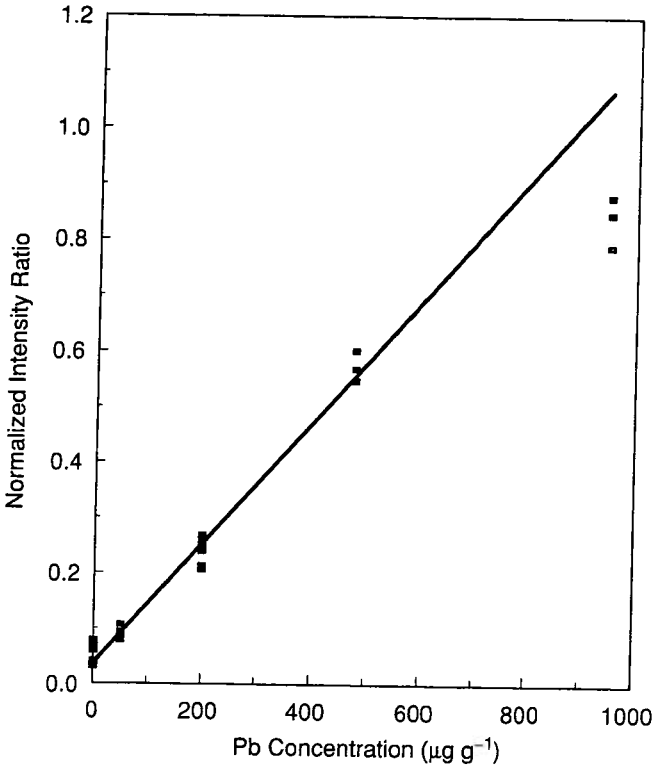

Figure 18.17. Ratio of the intensity of the lead line at 405.78 nm to that of the iron line at 404.58 nm as a function of the concentration of lead in loose Andover soil. The results show good linearity up to 500 mg Pb per kilogram of soil, but some fall-off in response at higher levels.

which is the 20 × 5 mg kg^{-1} TCLP limit). Soils having lead concentrations so high that remediation is necessary are easily identified, even though the exact concentration may not be accurately measured by the standard addition.

Analysis of the San Joaquin SRM material for lead was performed in the same manner as the Andover soil: that is each data point from the SRMs represents the average of 10 successive spectra, each made up of two spark events. Using loose soil (the pelletized SRMs exhibited an even greater signal drop than the pelletized Andover soil) and the standard addition technique, we took three sets of spectra for each sample concentration. Figure 18.18 shows a graph of the ratio of the intensity of the lead line at 405.78 nm to the iron line at 406.4 nm as a function of lead added to the San Joaquin soil sample. The data exhibit good linearity and low scatter. The original concentration of lead in the soil can be inferred from the ratio at the intercept at zero added lead to the slope of the standard addition curve. This value is 41 ± 18 mg Pb per kilogram of soil. This value is about a factor of 2 larger than the certified value of 19 mg Pb per kilogram of soil but does agree within our measurement uncertainty.

Comparing the San Joaquin reference material with the Andover soil illustrates the effect of iron content on instrument response. The slopes of the standard addition curves of the

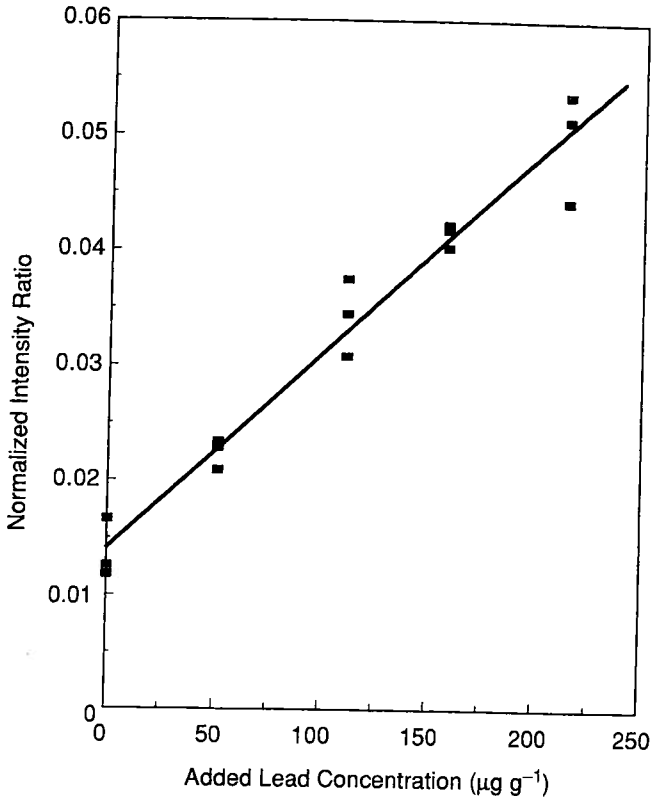

Figure 18.18. Ratio of the intensity of the lead line at 405.78 nm to that of the iron line at 406.36 nm as a function of lead concentration in San Joaquin soil (SRM 2709).

Andover soil and of the San Joaquin SRM, that is the ratio of the intensity of the lead line at 405.78 nm to the iron line at 406.4 nm, are 3.2×10^{-4} (intensity ratio/(milligrams of Pb per kilogram of soil)) and 9.8×10^{-4} (intensity ratio/(milligrams of Pb per kilogram of soil)), respectively. This difference is caused by the different iron concentrations in these samples (0.8% versus 3.3%).

The Montana SRM has a very high certified value for lead (5%). It is quite clear from the spectrum (Figure 18.19) that the lead feature is dominant. The intensity of the lead line at 405.78 nm is comparable to those of the iron lines in this sample.

Because of the very similar iron content of the two SRMs, we could estimate the lead content of the Montana soil using the San Joaquin soil standard addition curve. This procedure results in an estimate 4700 mg Pb per kilogram of soil for the Montana soil (certified value is 5532 mg kg^{-1}). Our estimate is within 15% of the NIST value, thus demonstrating the potential of the SIBS technology as a quick screening tool.

We also used SIBS to test soil for chromium. The spectra of samples with and without added chromium are shown in Figure 18.20. Figures 18.21–18.23 show standard addition curves for chromium in Andover soil, San Joaquin and Montana SRMs, respectively. The graphs indicate original chromium concentration in each soil of 18 ± 27 mg Cr per kilogram

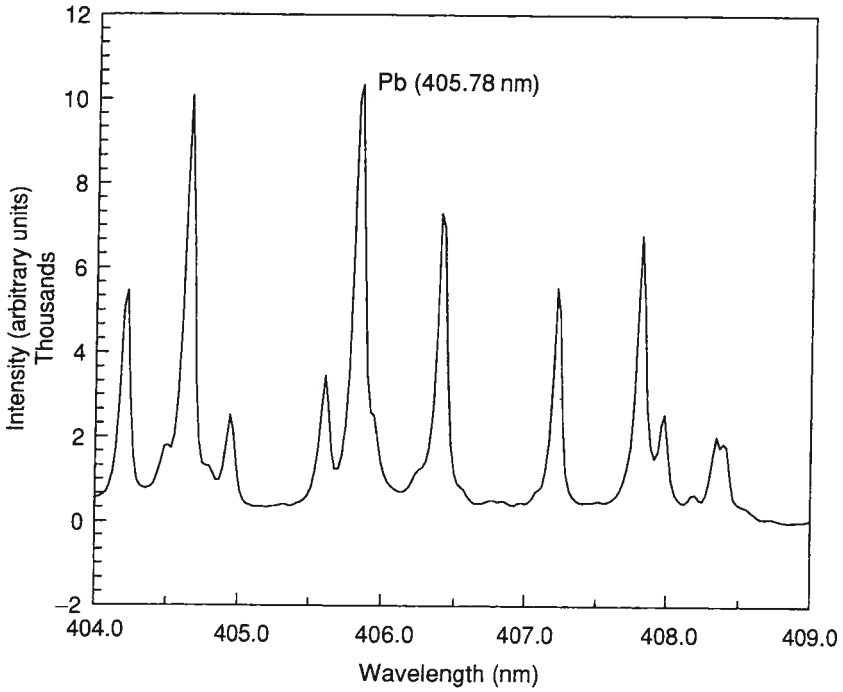

Figure 18.19. Spectrum of Montana SRM (2710) showing a very intense emission from lead at 405.78 nm.

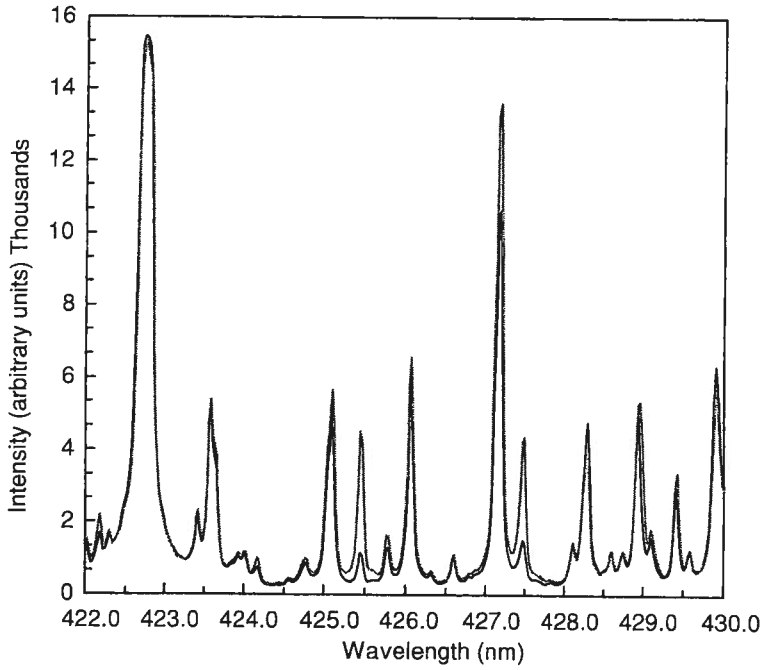

Figure 18.20. Spectra of Montana soil between 422 and 430 nm with (solid black line) and without (gray line) added chromium.

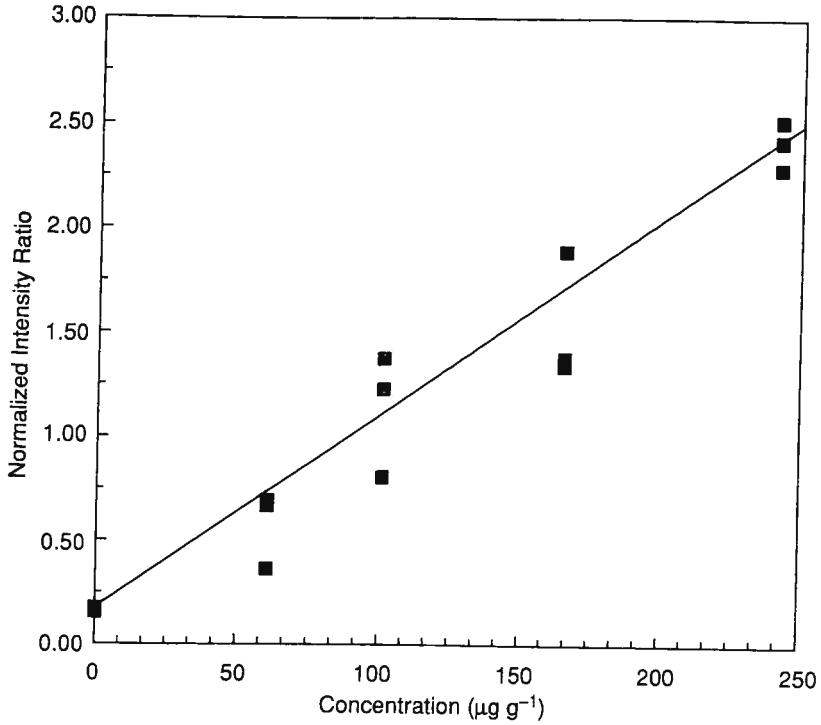

Figure 18.21. Ratio of the height of the chromium feature at 425.43 nm to that of the iron line at 426.06 nm as a function of added chromium in loose Andover soil.

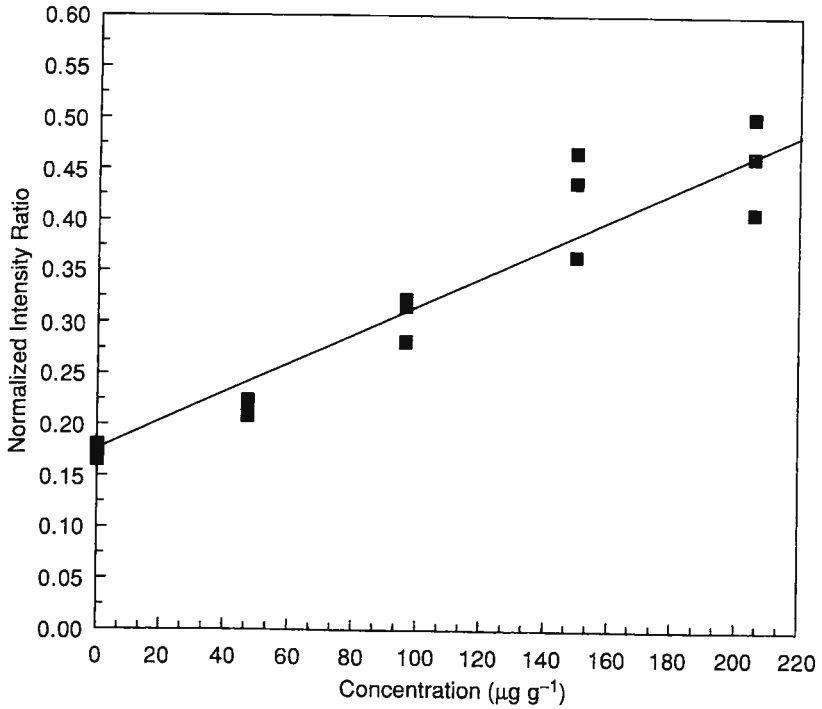

Figure 18.22. Ratio of the height of the chromium feature at 425.43 nm to that of the iron line at 427.15 nm as a function of added chromium in loose San Joaquin soil.

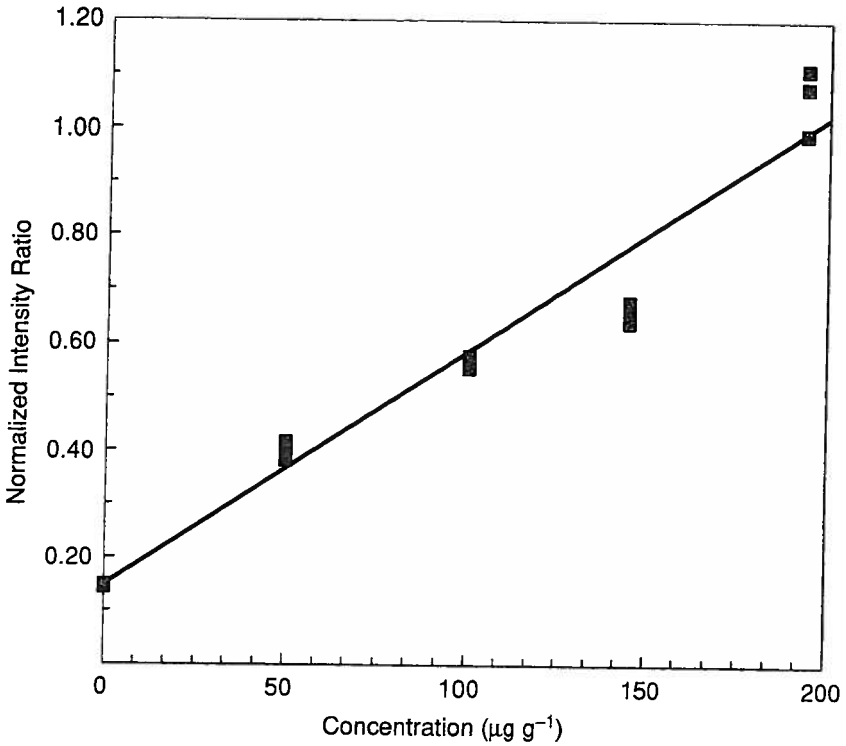

Figure 18.23. Ratio of the height of the chromium feature at 425.43 nm to that of the iron line at 427.15 nm as a function of added chromium in loose Montana soil.

of soil in the Andover soil, 111 ± 24 mg Cr per kilogram of soil in the San Joaquin soil and 33 ± 17 mg Cr per kilogram of soil for the Montana soil. These values compare with analyzed values of 14, 130, and 39 mg Cr per kilogram of soil, respectively for the Andover, San Joaquin and Montana soils. Certainly the agreement with the Andover soil is not statistically significant (the value is below the method detection limit), but the agreement with the other two samples is quite good.

Our present soil detection limits are 20 mg kg^{-1} for both Cr and Pb. These detection limits are worst-case values, stemming from the most difficult measurement situations examined during our preliminary studies. In sand, the detection limits are slightly lower. This is because of the homogeneous nature of sand, which makes it quite different from the other highly heterogeneous soils we tested. All the data on Pb and Cr are shown in Table 18.2.

These detection limits compare favorably with the detection limits for the X-ray fluorescence technique published in EPA Method 6200 [11]. In this document, "interference-free" limits (i.e. measured in quartz sand) are 150 mg kg^{-1} for Cr and 20 mg kg^{-1} for Pb. Actual repeated field-based detection limits varied substantially with the instrument used and ranged between 110 mg kg^{-1} and 900 mg kg^{-1} for Cr and between 40 mg kg^{-1} and 100 mg kg^{-1} and for Pb. To obtain these XRF detection limits, it was necessary to dry, grind and homogenize the samples. The SIBS method requires drying to provide a meaningful dry weight, but no other processing besides the application of the standard addition.

Table 18.2. *Certified values/lab measurements and SIBS values for Pb and Cr*

	SIBS analysis (mg kg^{-1})		Independent lab analysis (mg kg^{-1})		NIST certification (mg kg^{-1})	
Soil	Pb	Cr	Pb	Cr	Pb	Cr
Andover soil	32 ± 3[a]	18 ± 27	43 ± 4	14 ± 4	NA	NA
NIST SRM 2709 San Joaquin soil	41 ± 18	111 ± 24	< 4	73	18.9 ± 0.5	130 ± 4
NIST SRM 2710 Montana soil	4700	33 ± 17	5600	20	5532 ± 80	29[b]

[a] Lower error associated with increased number of averages.
[b] NIST analyzed, but not certified.

Compound sensitivity

During our development of SIBS for applications to metal-containing airborne particulate material, we have carefully evaluated the sensitivity of the method to different chemical formulations of the same analyte. We did this both for various forms of lead-bearing particulate (Pb, PbO, $Pb(NO_3)_2$) as well as for chromium aerosols of differing chemical identifies. In all cases, our SIBS-based measurements were in good agreement with the filter samples, which demonstrates that the chemical form of the metal does not influence the system response.

We have revisited this issue in developing SIBS for soils analysis because of a recent publication documenting such behavior in LIBS measurement of Ba, Cr and Pb in soil. In this publication, Cremers and co-workers doped soils to high levels (0.1%) with various lead and barium compounds [14, 15]. They reported a large amount of variability in signal intensity in the Pb(I) line at 405.8 nm (normalized to a Cr(I) line) in the compound series PbO, $PbCO_3$, $PbCl_2$, $PbSO_4$ and $Pb(NO_3)_2$. In their analysis, for example, lead chloride had three times the intensity of lead nitrate. This subsection documents preliminary efforts to uncover any changes in signal levels associated with chemical form. To date we have investigated this issue for soils containing two chemical forms of lead.

For the lead studies, we doped two samples of Andover soil at the 200 mg kg^{-1} level using two different lead compounds. ICP solutions of lead nitrate $Pb(NO_3)_2$ and lead chloride ($PbCl_2$) were used for this determination. These solutions were diluted with distilled water, quantitative aliquots were added to the soils, followed by drying, all in the manner described above. Following the sample preparation, the lead content of each sample was measured. The soils doped with lead nitrate and lead chloride had identical intensity ratios (Pb/Fe). We will address this important issue in more detail in future work.

Potential interference from organic contamination

In order to test the effects of organic contamination on the measurements, we divided a sample of soil which had been spiked previously with lead to a level of 225 mg Pb per

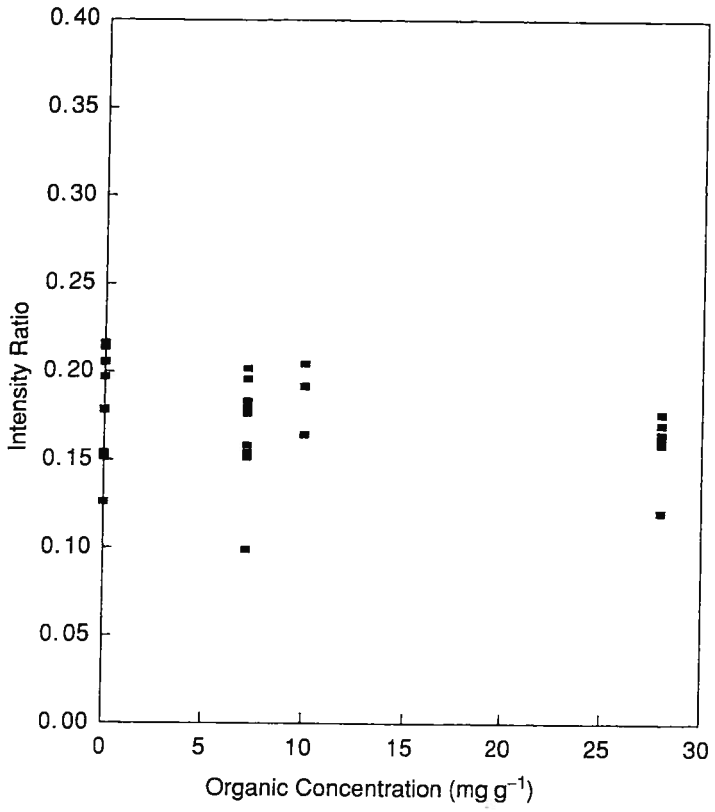

Figure 18.24. Ratios of the height of the lead feature at 405.78 nm to that of the iron feature at 404.58 nm in loose Andover soil with various quantities of organic contamination.

kilogram of soil into three portions. One we left alone, and the other two we spiked with organic material. After several measurements on one of the samples, we contaminated it further and made some additional determinations. The organic spiking procedure involved dissolving a measured amount of vacuum pump oil in trichloroethylene. Then, measured quantities of this solution were added to the previously weighed soil samples, the samples were thoroughly mixed and allowed to stand overnight at room temperature.

The results are shown in Figure 18.24, which displays repeated measurements of the ratio of the lead signal at 405.78 nm to that of the iron line at 406.36 nm as a function of organic contamination in the soil. Because of its high volatility and high surface area of the samples, we expect that most of the trichloroethylene evaporated from the samples prior to testing. Thus, the concentrations of organic contaminant shown in Figure 18.24 refer to the amount of pump oil added to the soil samples. Although the data are a bit more scattered than in some of our previous runs, they show that quite high levels of organic contamination do not interfere with the determination of lead in the sample. That is, within statistical uncertainties, ratios at all levels of organic contamination are the same. The total signal levels were reduced somewhat at higher levels of organic contamination, but the intensity ratios were not. Thus our technique is equally well suited to soils containing high levels of organic contamination as well as to those that are relatively clean.

Table 18.3. *Comparison of SIBS and LIBS*

	SIBS	LIBS
Excitation system	Electrical	Optical
Excitation power	1–6 J	75–350 mJ
Detection systems applied	Wavelength dispersive and filter based	Wavelength dispersive only
Development of fieldable system?	On-going	Accomplished
Detection limits (using Pb as an example)	In air 5 $\mu g\ m^{-3}$ In soil 25 $mg\ kg^{-1}$	In air 190 $\mu g\ m^{-3}$ [16] In soil 57 $mg\ kg^{-1}$ [15]
Standoff detection possible?	No	Yes

18.5 Discussion and future directions

The set of applications described here shows the wide range of utility of SIBS. SIBS can be applied both to the elemental analyses of airborne particulate material and to solids, both soils and powders. An advantage of SIBS in both of these arenas is the high-energy spark. The large amount of energy deposited allows a large plasma to be generated, which helps to ensure good sampling statistics and sampling in the aerosol monitoring case. For airborne particle analysis, there are definite advantages to using an electrically generated 5 J spark over an optically generated 100 mJ spark (these sources having similar cost). In the case where the possibility of spectral interference has been evaluated and is low, this energetic excitation source can be coupled with the simple and inexpensive interference filter and PMT detection. This results in a simple and easy-to-use, real-time air monitoring system that can be used to protect workers or optimize processes.

SIBS solids applications also benefit from the large and energetic excitation spark. In this case, it allows processing of a larger sample without changing spark characteristics. In soil sampling, we are able to achieve detection limits in 10 or 15 min that are nearly as sensitive and reproducible as an analytical lab using a process taking several hours per sample, not including sampling and transport time. This type of quick analytical instrumentation is highly desired as field-screening for toxic metals in soil. In order for the device to be sufficiently portable, we are currently working on hardware miniaturization of the soil system. Table 18.3 briefly compares the SIBS results discussed here with LIBS characteristics from literature. SIBS and LIBS are very similar in both results and application. The most important differences are the fact that LIBS can be used in a stand-off fashion and SIBS has a simpler and more energetic plasma source.

The authors acknowledge the contributions of the many people at PSI who have contributed to the development of SIBS. Most particularly, we would like to acknowledge Dr. Karl Holtzclaw and Dr. Mark Fraser, who made significant efforts early in the development

of SIBS. Additionally, we acknowledge the newer members of the SIBS team, Dr. Rick Wainner and Dr. Brian Decker, who have been involved in furthering the soil applications, and in the airborne lead monitor development, respectively. Dr. Steven Davis has been our constant supporter, both personally and professionally, and has our deep gratitude. This work has been funded by the US Department of Energy, US Environmental Protection Agency, US Army, and the National Institute of Occupational Safety and Health.

18.6 References

[1] R. M. Barnes (editor), *Emission Spectroscopy* (Stroudsburg, PA: Dowden, Hutchison & Ross, 1973).
[2] H. R. Griem, *Principles of Plasma Spectroscopy* (Cambridge: Cambridge University Press, 1997).
[3] M. N. Hirsch and H. J. Oskam (editors), *Gaseous Electronics, Volume 1: Electrical Discharges* (New York: Academic Press, 1978).
[4] J. M. Meek and J. D. Craggs (editors), *Electrical Breakdown of Gases* (New York: John Wiley and Sons, 1978).
[5] R. Payling, D. G. Jones and A. Bengtson (editors), *Glow Discharge Optical Emission Spectroscopy* (Chichester: John Wiley and Sons, 1997).
[6] L. J. Radziemski and D. A. Cremers, Spectrochemical analysis using laser plasma excitation. In *Laser Induced Plasmas and Applications*, L. J. Radziemski and D. A. Cremers (editors), chapter 7 (New York: Marcel Dekker, 1989), p. 295.
[7] R. N. Berglund and B. Y. Liu, *Anal. Chem.*, **7** (1973), 147.
[8] J. Zynger and S. R. Crouch, *Appl. Spectrosc.*, **29** (1975), 244.
[9] *Hexavalent Chromium in Workplace Atmospheres* (OSHA Method No. ID-215) (Salt Lake City, UT: OSHA, 1998).
[10] M. Martin and M.-D. Cheng, *Appl. Spectrosc.*, **54** (2000), 1279.
[11] Code of Federal Regulations, Title 40, Volume 17, Parts 266–299, 40CFR266, pp. 5–119, *Standards for the Management of Specific Hazardous Wastes and Specific Types of Hazardous Waste Management Facilities*, Revised as of July 1, 1997.
[12] US Environmental Protection Agency, Method 6200, *Field Portable X-Ray Fluorescence Spectrometry for the Determination of Elemental Concentrations in Soil and Sediment*, Revision 0, January 1998.
[13] US Environmental Protection Agency, Method 4500, *Mercury in Soil by Immunoassay*, Revision 0, January 1998.
[14] M. E. Fraser, T. Panagiotou, A. J. R. Hunter *et al.*, *Plating and Surface Finishing*, **87** (2000), 82.
[15] A. S. Eppler, D. A. Cremers, D. D. Hickmott, M. J. Ferris and A. C. Koskelo, *Appl. Spectrosc.*, **50** (1996), 1175.
[16] B. T. Fisher, H. A. Johnsen, S. G. Buckley and D. W. Hahn, *Appl. Spectrosc.*, **55** (2001), 1312.